Water—substrate physico-chemistry in wetting dynamics

Petter Johansson¹, Andreas Carlson^{2,3} † and Berk Hess¹ ‡

¹Department of Theoretical Physics and Swedish e-Science Research Center, KTH Royal Institute of Technology, 10691 Stockholm, Sweden

²John A. Paulson School of Engineering and Applied Sciences and Wyss Institute for Biologically Inspired Engineering, Harvard University, Cambridge, MA 02138, USA.
³Department of Mathematics, University of Oslo, 0316 Oslo, Norway.

(Received ?; revised ?; accepted ?. - To be entered by editorial office)

We consider the wetting of water droplets on substrates with different chemical composition and molecular spacing, but with an identical equilibrium contact angle. A combined approach of large-scale molecular dynamics simulations and a continuum phase field model allows us to identify and quantify the influence of the microscopic physics at the contact line on the macroscopic droplet dynamics. We show that the substrate physico-chemistry, in particular hydrogen bonding, can significantly alter the flow. Since the material parameters are systematically derived from the atomistic simulations our continuum model has only one adjustable parameter, which appears as a friction factor at the contact line. The continuum model approaches the atomistic wetting rate only when we adjust this contact line friction factor. However, the flow appears to be qualitatively different when comparing the atomistic and continuum model, highlighting that non-trivial continuum effects can come into play near the interface of the wetting front.

Key words: contact lines, non-continuum effects, molecular dynamics, phase field theory, numerical simulations

1. Introduction

The study of wetting has a history stretching back more than two centuries, when the equilibrium drop shape on a substrate was described by the three-phase surface energies (Young 1805). Wetting dynamics, on the other hand, have proven to be more challenging to describe (de Gennes 1985; Bonn et al. 2009), as the hydrodynamic description is incomplete at the contact line (where the vapour–liquid–solid phases meet) with a diverging viscous stress (Huh & Scriven 1971; Voinov 1976).

Several theories have been proposed to relax this contact line singularity, e.g. a slip length (Tanner 1979; de Gennes 1985; Ren et al. 2010), interfacial diffusion (Jacqmin 2000; Qian et al. 2003; Carlson et al. 2009; Yue et al. 2010; Carlson et al. 2011) and molecular stochasticity/kinetics (Blake & Haynes 1969; Davidovitch et al. 2005), all of which have been demonstrated to rationalise different experimental observations. Since it is challenging to characterise the contact line singularity in macroscopic experiments these theories often rely on ad-hoc parameters and its precise physical nature is still debated (Bonn et al. 2009).



2

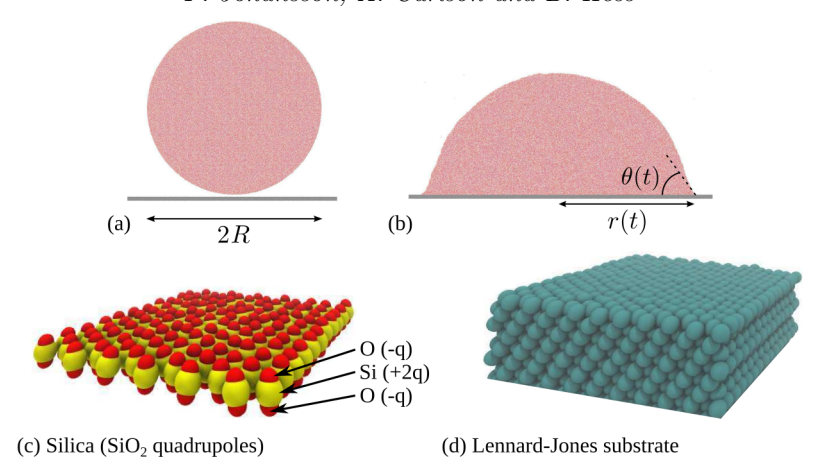


FIGURE 1. a) Initial condition of the quasi-2D simulations, where a water droplet with radius R is brought in contact with a solid substrate. b) At time t>0 after droplet—substrate contact the droplet spreads onto the substrate with a growing wetting radius r(t) and a dynamic contact angle $\theta(t)$. c) The molecular structure of a silica-like substrate that consists of hexagonally packed rigid SiO₂ quadrupoles. q denotes the atomic charge. d) A substrate of closely packed Lennard-Jones atoms. Note that the solid substrates illustrated in c) and d) have the same equilibrium contact angle $\theta_0=37^\circ$ when wetted by water.

Particle based approaches such as molecular dynamics (MD) alleviate the need for boundary conditions at the contact line and allow a detailed study of the dynamics of single molecule interactions. Over the last decades MD has become an important complement to macroscopic modelling (Koplik et al. 1988; Thompson & Robbins 1989; Gentner et al. 2003; Qian et al. 2004), in particular as it allows modelling of the nanoscopic physics at the contact line. Studies of wetting using MD have mostly been limited by the available computational power, with system sizes a few times larger than the typical interaction interaction range between molecules of 1 nm (Liu et al. 2010; Ho et al. 2011; Ritos et al. 2013), which may lead to finite size effects on the results. Many studies have also been limited to monatomic systems (Thompson & Robbins 1989; Qian et al. 2003; De Coninck & Blake 2008; Winkels et al. 2012; Nakamura et al. 2013), while more experimentally realistic systems e. g. water on a silica, have primarily focused on equilibrium material properties (Lee & Rossky 1994; Werder et al. 2003; Janeček & Netz 2007).

In order for a molecular description to mimic an experimental system we must account for the molecular structure and interactions of real liquids and solids. Moreover, the droplet size must be significantly larger than the intermolecular interaction range to avoid the influence of finite size effects on the dynamics. We describe below the wetting dynamics of such a system by deploying a multi-scale approach composed of a combination of large-scale MD and macroscopic phase field (PF) simulations in quasi-2D. The initial droplet shape and the dynamic wetting process is illustrated in figure 1a-b, which we investigate on a silica-like substrate with surface charges (figure 1c) and two less realistic Lennard-Jones (LJ) substrates: A substrate consisting of (non-charged) Lennard-Jones atoms (figure 1d) and a pure Lennard-Jones potential wall. All substrates have the same surface energy, allowing us to quantify the influence of the molecular substrate composition on the wetting dynamics. Moreover, we show that the electrostatic interactions between molecules can generate non-trivial effects at the interface, which alters the dynamics of spreading and limits the molecular motion at the contact line.

Parameter	Symbol	Value	Number	Symbol	Relation	Value
Viscosity	μ	$8.77 \times 10^{-4} \text{Pa s}$	Reynolds	Re	$\frac{\rho \gamma R}{r^2}$	3.7
Density	ρ	986 kg m^{-3} $2.29 \times 10^{-9} \text{ m}^2 \text{ s}^{-1}$	Ohnesorge	Oh	$Re^{\frac{\rho\gamma R}{\mu^2}}$	0.52
Diffusion coefficient Surface tension (LV)	$D \sim \gamma$	$2.29 \times 10^{-8} \text{ m/s}$ $5.78 \times 10^{-2} \text{ Pa m}$	Péclet	Pe	$\frac{\frac{\gamma R}{D\mu}}{\frac{\epsilon}{R}}$	1400
Interface width (LV)	ϵ	0.75 nm	Cahn	C_n	$u_{\alpha_{l}}^{\epsilon}$	0.015
Initial droplet radius	R	50 nm	Contact line friction	μ_f	$\frac{\mu}{\mu}$	0–300
Contact line friction	Hel	$(0-3) \times 10^{-1} \mathrm{Pas}$	111001011			

Table 1. Left: Material properties measured from equilibrium MD simulations. The values for the surface tension γ and interface width ϵ are for the liquid–vapour (LV) interface. Right: Scaling analysis gives several non-dimensional numbers, describing the ratios between different physical time and length scales of the wetting dynamics.

2. System parameters, material properties and dimensional analysis

The droplet dynamics can be limited by different physical mechanisms and to estimate these we begin by measuring the bulk macroscopic material parameters of our molecular system, which is the principal input to our continuum model, described further down.

Water is described by the 3-site SPC/E model (Berendsen et al. 1987), which is computationally efficient and models the molecular dipole moment. Its relevant liquid properties are listed in table 1, as measured using equilibrium MD simulations with particle-mesh Ewald (PME) electrostatics (Essmann et al. 1995), as described in the next section. The interface thickness is characterised as the length over which the liquid changes to the vapour density.

There are different time scales which can describe the droplet dynamics of a wetting experiment. Scaling analysis identifies a viscous time $\tau_{\mu} \equiv \mu R/\gamma = 0.76\,\mathrm{ns}$, an inertial time $\tau_{\rho} \equiv \sqrt{\rho R^3/\gamma} = 1.5\,\mathrm{ns}$ and a diffusive time $\tau_{D} \equiv R^2/D = 1.1\,\mu\mathrm{s}$ (see table 1 for parameter values). The relation between these time scales give us some information about our model system: Since $\tau_{D} \gg \tau_{\mu}, \tau_{\rho}$ the dynamics are not believed to be limited by diffusion. Furthermore, these time scales form several non-dimensional numbers: The Ohnesorge number $Oh \equiv \tau_{\rho}/\tau_{\mu} = \mu/\sqrt{\rho\gamma R} = 0.52$ gives the ratio of inertia–capillary and viscous effects and the Péclet number $Pe \equiv \tau_{\mu}\tau_{D} = \gamma R/D\mu = 1400$ gives the ratio of advection and diffusion. By interpreting the characteristic speed as $U_c \equiv \gamma/\mu$ we get the ratio between viscous and inertial forces as the Reynolds number $Re \equiv \rho U_c/\mu = \rho \gamma R/\mu^2 = Oh^{-2} = 3.7$. Since $Oh \sim Re \sim 1$ our system is in a regime where both inertial and viscous forces are important.

Two additional non-dimensional numbers appear in the phase field model. The Cahn number $C_n \equiv \epsilon/R$ gives the ratio between the interface thickness ϵ and the initial droplet radius R, and $\mu_f \equiv \mu_{cl}/\mu$ is the ratio between a contact line friction parameter μ_{cl} and the viscosity.

We scale the governing equations and the results as: $\hat{x} \equiv \frac{x}{R}$, $\hat{y} \equiv \frac{y}{R}$, $\hat{r} \equiv \frac{r}{R}$, $\hat{t} \equiv \frac{t}{\tau_{\mu}}$, $\hat{p} \equiv \frac{p\tau_{\mu}}{\mu}$, $\hat{\phi} \equiv \frac{\phi\epsilon}{\gamma}$, where x,y are the system coordinates, r=r(t) the wetted radius, t the time, p=p(x,y,t) the pressure and $\phi=\phi(x,y,t)$ the chemical potential. (^) denotes a non-dimensional variable.

Type	Atom (Pair)	m(u)	q(e)	σ (nm)	$\varepsilon (\mathrm{kJ} \mathrm{mol}^{-1})$		
Water	$_{ m H}$	1.00	0.42	0.0	0.0	a	5 ()
	O	16.00	-0.85	0.32	0.65	Substrate	δ (nm)
Silica	Si	0.0	1.34	0.45	0.2	Silica	0.0(0)
	O	16.00	-0.67	0.32	0.65	LJ Atom.	1.1(1)
LJ Atom.	LJ	63.55	0.0	0.24	10.00	LJ Pot.	Infinite
	LJ–O			0.28	1.77		
L.I.Pot	L.I–O			0.28	1.86		

Table 2. Left: Interaction parameters for a generic LJ substrate atom and the interaction parameters bond length σ , energy ϵ , between different atom types are calculated using Lorentz–Berthelot combination rules. The LJ–O interactions of the potential and atomistic LJ substrates gives an equilibrium contact angle $\theta_0 = 37^{\circ}$. Right: Slip length δ measured in MD simulations of water as a function of substrate composition, where the number in the parentheses denote the error.

3. Simulation set-up

3.1. Atomistic description: Molecular dynamics

We consider the wetting of water molecules on three different substrates: A substrate constructed by an integrated Lennard-Jones (LJ) 10–4 potential wall, a "rough" fcc structure (111 interface) of LJ atoms with a spacing of 0.27 nm (figure 1d) and a semi-realistic silica that consists of a monolayer of rigid SiO₂ quadrupoles set in a hexagonal formation with a spacing of 0.45 nm (figure 1c). The silica differs from the LJ substrates by the ability to form hydrogen bonds with water, which limits the molecular motion on the substrate. The three substrates can be interpreted in terms of the liquid–surface friction, from none (10–4 LJ potential), to intermediate (LJ atomistic) and high (silica). The substrates are atomistically smooth and the 10–4 LJ potential wall interaction is described by

$$U = 2\pi \varepsilon n \left(\frac{\sigma^6}{h^4} - \frac{2\sigma^{12}}{5h^{10}} \right) \tag{3.1}$$

where U is the interaction potential, $n=16~\mathrm{nm}^{-2}$ is the area number density of integrated virtual LJ atoms, h is the height of an interacting atom above the wall and ε and σ are Lennard-Jones potential parameters denoting the energy minimum and the bond distance between interacting particles.

To maintain the same equilibrium angle $\theta_0=37^\circ$ on all substrates, we adjusted the liquid–solid interaction strengths that are directly related to the surface energies in the system. These energies are related to θ_0 through Young's equation $\gamma\cos\theta_0=\gamma_{SV}-\gamma_{SL}$, where $\gamma\equiv\gamma_{LV},\gamma_{SL},\gamma_{SV}$ are the liquid–vapour (LV), solid–liquid (SL) and solid–vapour (SV) surface tensions. The molecular interaction parameters of the substrates that yield θ_0 were determined by measuring the contact angle of small water droplets at equilibrium on the substrates. The final parameters are listed in table 2 for PME electrostatics. By keeping θ_0 fixed we reduce our parameter space, allowing us to investigate the principal influence of the atomistic composition of our substrates on the wetting dynamics independent of surface energetics.

To characterise the different substrates on the continuum length scales we measure their slip lengths δ . This property appears in the Navier boundary condition and quantifies the tendency of a liquid to flow along a substrate (Bachelor 1967). The slip lengths of our atomistic substrates were measured using a Couette flow and are reported in table 2. Since the potential LJ substrate is frictionless it has an infinite slip length.

The quasi-2D droplet cylinder has a periodic width of 4.67 nm and a radius R of 50 nm,

Material	Property	PME	RF
Water	$\gamma (10^{-2} \text{Pa m})$	5.84	5.33
Silica	$q_{\mathrm{Si}}\left(e\right)$	1.34	1.32
	$q_{\rm O} \; (e)$	-0.67	-0.66
LJ Atom.	$\varepsilon (\mathrm{kJ} \mathrm{mol}^{-1})$	1.77	1.76
LJ Pot.	$\varepsilon (\mathrm{kJ} \mathrm{mol}^{-1})$	1.86	1.86

Table 3. Material parameters of the MD systems with PME and RF treatments of the electrostatics. To keep the equilibrium contact angle fixed $\theta_0 = 37^{\circ}$ the molecular interaction parameters of the substrate atoms are slightly adjusted for PME. The water liquid–vapour surface tension changes by around 10 % when comparing PME with the RF, while all other bulk properties are insensitive to the treatment of the electrostatics.

in total consisting of 1.2 million water molecules. Before it is brought in contact with the substrate, the droplet is equilibrated at a temperature T of 300 K by deploying a stochastic dynamics integrator with periodic boundary conditions to mimic an infinite quasi-2D system. After the initial equilibration, a leap-frog integrator was used for the time marching. To mimic the energy dissipation into a large substrate, we coupled the substrate atoms to a velocity rescaling thermostat, dissipating thermal energy using a 10 ps coupling time. The water molecules were not coupled to a thermostat. The electrostatic forces between the partial charges were calculated using the particle-mesh Ewald (PME) method that takes the Coulomb interactions between all charges in the system into account. In addition, we have tested a simplified approach using reaction-field (RF) electrostatics with a cut-off of 0.9 nm. Beyond the cut-off this treatment assumes a dielectric medium with infinite dielectric constant, which leads to a linear reaction force to the Coulomb potential. The RF treatment is mainly used due to its computational efficiency as it scales linearly with the number of atoms N compared $N \log N$ for the PME treatment. RF simulations give good results for systems with molecules that have zero net charge, which is valid here. However, it also requires a high dielectric constant, which is not true for our droplets since we have both a liquid and a vapour phase. Among the measured equilibrium properties reported in table 1 only the surface tension coefficient γ is affected by the electrostatics treatment, decreasing by ≈ 10 % for the RF compared to the PME prediction. This decrease is related with an overestimation of the surface dipole (surface charge) with the RF treatment, due to favourable interactions between water molecules and the artificial dielectric medium in the vapour phase. Note that any effect on the scale the surface dipole is absent in the continuum model that we introduce later, but we do not expect this to affect the model. To maintain the same equilibrium contact angle $\theta_0 = 37^{\circ}$ the water–substrate interaction parameters were slightly adjusted for the RF simulations compared to the PME values reported in table 3.

The MD simulations were performed using Gromacs 5.0.3 (Abraham *et al.* 2015) in double precision and with a time step of 2 fs. Every 0.01 ps flow data was collected in bins of size $0.25 \times 0.25 \,\mathrm{nm^2}$, then averaged every 1000 collection points to create 2D maps of mass flow, temperature and atom density with a temporal resolution of 10 ps. The simulations were run on the supercomputers Triolith at Linköping University and Beskow at the Royal Institute of Technology, Sweden. We simulated droplets composed of 1.2 million water molecules (3.6 million atoms) for ≈ 8 ns, which on 640 cores took 2 days for PME and 1 day for RF electrostatics.

3.2. Continuum description: Phase field model

To understand the link between the molecular contact line physics and the macroscopic droplet dynamics, we couple the MD description with a continuum phase field (PF) model, described further by Carlson et al. (2011). The PF model is based on a phenomenological description of the free energy of the system F = F(x, y, t) (Jacqmin 2000), which is a function of the non-dimensional concentration $\hat{C} = \hat{C}(x, y, t)$ of the two phases considered interpreted as liquid $\hat{C} = 1$ and vapour $\hat{C} = -1$. These two phases are represented by the two minima in the bulk free energy $\Psi(\hat{C}) \equiv (\hat{C} + 1)^2 (\hat{C} - 1)^2 / 4$. By assuming that a variation in concentration \hat{C} is balanced by a flux, represented by the gradient of the chemical potential $\delta \hat{F}/\delta \hat{C}$, gives the Cahn–Hilliard equation (Cahn & Hilliard 1958), represented here in a non-dimensional form,

$$\frac{\partial \hat{C}}{\partial \hat{t}} + \hat{\mathbf{u}} \cdot \nabla \hat{C} = \frac{1}{Pe} \nabla \cdot \left(\nabla \frac{\delta \hat{F}}{\delta \hat{C}} \right) = \frac{1}{Pe} \nabla \cdot \left(\nabla \left(\beta \Psi'(\hat{C}) - C_n^2 \nabla^2 \hat{C} \right) \right) . \tag{3.2}$$

 $C_n^2 \nabla^2 \hat{C}$ represents the energy cost of having an interface and $\hat{\mathbf{u}}$ is the non-dimensional velocity. A no-flux boundary condition is used for the chemical potential $\nabla \hat{\phi} \cdot \mathbf{n} = 0$, where \mathbf{n} is the boundary normal. $\nabla \hat{C} \cdot \mathbf{n} = 0$ is used for the sides of the domain in contact with ambient air and along the symmetry line. At the solid substrate we use the non-equilibrium wetting boundary condition (Carlson *et al.* 2009, 2011)

$$\mu_f C_n \left(\frac{\partial \hat{C}}{\partial \hat{t}} + \hat{\mathbf{u}} \cdot \nabla \hat{C} \right) = -C_n \nabla \hat{C} \cdot \mathbf{n} + \cos \theta_0 g'(\hat{C}), \qquad (3.3)$$

where $g(\hat{C}) \equiv (-\hat{C}^3 + 3\hat{C} + 2)/4$ is a function varying the surface energy for a wet or dry substrate. The left-hand side of 3.3 allows for local deviations from equilibrium. μ_f is a scaled phenomenological contact line friction parameter and sets the time scale for the local relaxation of the interface to form the equilibrium contact angle θ_0 at the substrate.

Since Re is close to unity, viscous and inertial effects are of similar importance for the flow, which is described by the non-dimensional continuity and Navier–Stokes equations

$$\nabla \cdot \hat{\mathbf{u}} = 0, \tag{3.4}$$

$$\hat{\rho}(\hat{C})Re\left(\frac{\partial \hat{\mathbf{u}}}{\partial \hat{t}} + \hat{\mathbf{u}} \cdot \nabla \hat{\mathbf{u}}\right) = -\nabla \hat{p} + \hat{\mu}(\hat{C})\nabla \cdot \left(\nabla \hat{\mathbf{u}} + \nabla \hat{\mathbf{u}}^T\right) + \frac{\hat{\phi}\nabla \hat{C}}{C_n}, \quad (3.5)$$

where \hat{p} is the pressure and $(\hat{\phi}\nabla\hat{C})/C_n$ represents the surface tension force. The density is a function of the different phases and described as $\hat{\rho}(\hat{C}) = \frac{1}{2}(1+\hat{C}) + \frac{\rho_g}{2\rho}(1-\hat{C})$ with ρ being the liquid density and $\rho_g = 10^{-3}\rho$ the vapour density. We use a similar functional form for the viscosity $\hat{\mu}(\hat{C}) = \frac{1}{2}(1+\hat{C}) + \frac{\mu_g}{2\mu}(1-\hat{C})$ with μ as the liquid viscosity and $\mu_g = 0.02\mu$ the vapour viscosity. The droplet is assumed to be at ambient constant pressure $(\hat{p} = 0)$.

Since there is molecular motion along the solid substrate we use a Navier slip condition for the velocity at the solid substrate

$$\nabla \hat{\mathbf{u}} \cdot \mathbf{n} = \lambda \hat{u}_s \,, \tag{3.6}$$

where $\lambda \equiv R/\delta$ is the non-dimensional slip length and \hat{u}_s is the computed slip velocity at the substrate.

Together, the coupled Cahn–Hilliard and Navier–Stokes equations represent a phenomenological and isothermal model for the description of droplet spreading of an incompressible liquid. Following Carlson *et al.* (2009, 2011) equations 3.2–3.6 are solved

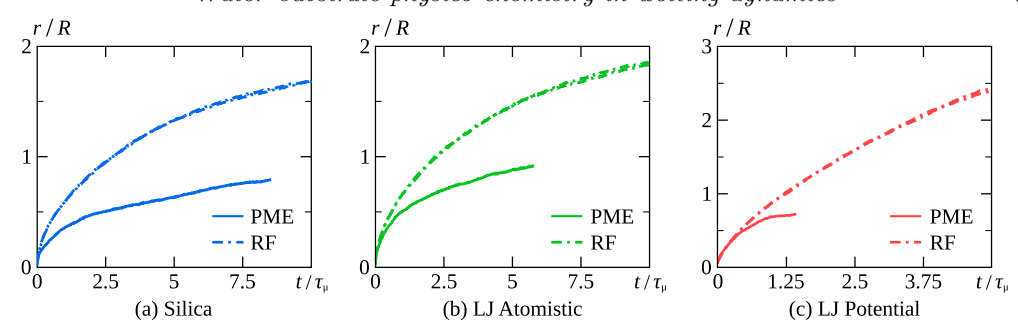


FIGURE 2. Spreading radius r(t) measured from MD simulations of water droplets with PME and RF electrostatic treatment for the (a) silica, (b) atomistic LJ and (c) LJ potential substrates. Each figure contains two different simulations and the curves for r(t) are coincident. Although the equilibrium contact angle θ_0 is fixed, it is clear that there is a large influence of the substrate physico-chemistry. In addition, we observe that the electrostatic treatment of the water molecules can significantly influence the spreading dynamics, where the full electrostatics (PME) predicts a spreading rate 2–4 times slower than the reaction-field (RF).

using a finite element method with a mesh size $C_n/8$ and with the measured material properties from our equilibrium MD simulations (tables 1 and 2). Our continuum model has only one free parameter: the scaled contact line friction factor μ_f . To illustrate the shape of the droplet and the position of the moving contact line we define the interface along the contour of $\hat{C} = 0$.

Having thus defined the atomistic and continuum description of the wetting process, we want to characterise the mechanisms dominating the wetting dynamics by comparing the computed dynamics. In particular, we want to see if the continuum contact line friction parameter μ_f adequately captures the molecular processes at the contact line as a function of the substrate composition.

4. Droplet spreading dynamics

4.1. Substrate physico-chemistry and electrostatic interactions

We begin by analysing the wetting dynamics of the MD model to characterise the influence of our different substrates and the electrostatics treatment. Two measures of the global dynamics of a wetting experiment are the wetting radius r(t) and the droplet interface shape. These measures are shown in figure 2 and 3 for all three substrates using both of the electrostatics treatments. Although all systems have similar equilibrium properties, we see a large influence on the wetting dynamics as a function of the substrate physico-chemistry and the electrostatics treatment.

We will first focus on the influence of the substrate compositions, returning to the difference between PME and RF electrostatics further on. We see that the contact line speed increases with the measured slip length δ (table 2), as the viscous resistance close to the substrate is reduced. Hydrogen bonds can form between water and substrate molecules on the silica, resulting in slower wetting compared to the LJ substrates. Even the organisation of LJ atoms in the substrates can greatly influence the dynamics, as we observe a more rapid wetting on the frictionless LJ potential compared to the atomistic substrates. For the PME spreading curves (figure 2) we see a transition from a $r(t) \propto t^{1/2}$ regime to a slower regime, while for RF there is no clear transition within the time simulated. The droplet shapes (figure 3) show that the speed at which a meniscus is formed also is related to the viscous friction, a process that is very slow on the silica

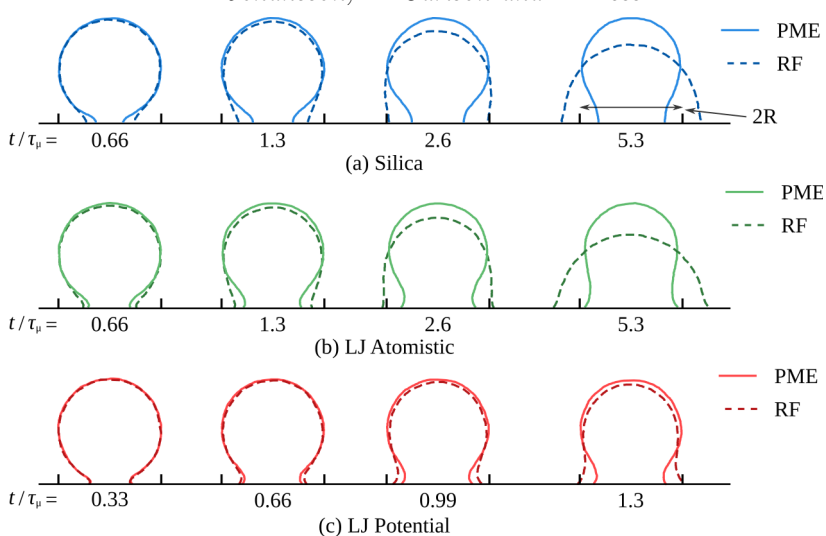


FIGURE 3. Droplet shapes from the MD simulations with different electrostatics treatments, as they spread on three substrates with different composition. The electrostatic treatment only affects the long-time regime, when r/R > 0.5, and the water–substrate physico-chemistry affects both the spreading rate and the dynamic droplet shape. The interface is extracted at the half-density contour of the droplet.

substrate compared to either of the LJ substrates. Thus, we see a large influence of substrate physico-chemistry on both of our selected measures of the wetting dynamics. In all simulations we observe local temperature increase of the liquid at the contact line, which scales with the contact line speed. However, this increase is never more than a few percent and is believed to have a negligible influence on the spreading dynamics.

To understand how the flow affects the droplet shape, we have extracted the flow field from the PME simulations, since this is the closest description of a real water system. Time-averaged flow fields close to the contact line are presented in figure 4 for an early regime where r/R = 0.2 and a later regime where r/R = 0.8. On the silica we observe that at early times there is a significant amount of fluid transported to the contact line along the droplet interface, not from the centre bulk of the droplet. In contrast, the flow becomes more parallel to the substrate at later times. On the LJ substrates the initial regime also entail some transport of fluid from the droplet interface, but it small compared to the flow from the centre (bulk) of the drop created by the increased substrate slip.

To further characterise the difference in the fluid motion in these regimes, we extract path traces of molecules attached at the contact line on the silica in the two different regimes (figure 5). Our analysis corroborates the flow fields in figure 4, suggesting different physical mechanisms of contact line advancement. In the early regime most molecules approach the contact line through an advective flow. In contrast, the later regime shows that the contact line largely advances by molecules detaching from the substrate and attaching a single lattice spacing ahead of it. Thus the main mode of contact line advancement in the slow regime appears to be diffusive. Note that the initial speed of the droplet as it comes in contact with the substrate is much lower than the wetting speed and does not influence our results.

There is a salient point we wish to highlight in these results. Our simulations resemble some of the regimes that have previously been identified in wetting dynamics and we see that they correspond well to two different exponents for the wetting rate $r(t) \propto t^k$,

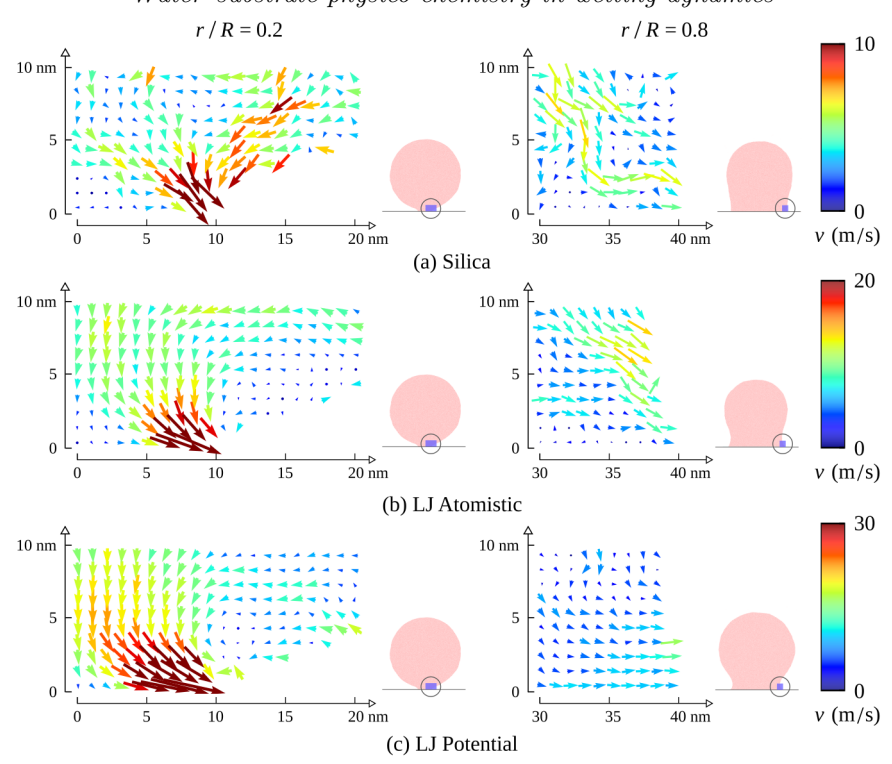


FIGURE 4. The flow field near the contact line extracted from the MD simulations for r/R of 0.2 (left) and 0.8 (right), time averaged over 200 ps. At short times liquid molecules are transported to the contact line from above, near the droplet interface. At long times, the flow has changed characteristics and is parallel with the substrate. We note that the droplet spreading on the silica substrate is about half as fast as on the atomistic LJ substrate, and a third as fast as on the potential LJ substrate.

illustrated in figure 6. The short time dynamics $k \ge 1/2$ indicate inertial effects (Bonn et al. 2009) or possibly a slip flow Nakamura et al. (2013), while the late time spreading rate has a smaller power $k \approx 1/3$ but does not follow the classical Tanner's law which in 2D gives $r(t) \propto t^{1/7}$ (Tanner 1979; de Gennes 1985). However, fluctuations (Davidovitch et al. 2005) could shift the power-law dependence from $r \propto t^{1/7}$ to $r \propto t^{1/4}$. The molecular motion in the late time regime could resemble the phenomenological molecular kinetic theory Blake & Haynes (1969), which advances the contact line by molecules jumping between potential wells on the substrate. The predicted contact line velocity $v_{\rm MKT} =$ $2 \kappa^0 \Lambda \sinh \left(\frac{\gamma(\cos \theta_0 - \cos \theta)}{2 n k_B T} \right)$ is independent of the flow in the drop and is instead related to the dynamic contact angle θ , a molecular jump rate κ^0 , a displacement length Λ , the site number density n and the thermal energy k_BT . We can estimate the values for these parameters from the PME MD simulations on silica as on average 2 water molecules form hydrogen bonds with one substrate oxygen molecule, which sets the number density as $n = 11.4 \,\mathrm{nm}^{-2}$. These hydrogen-oxygen bonds between water and substrate molecules form and break at a rate of $\kappa^0 \approx 0.1\,\mathrm{ps^{-1}}$ measured in an equilibrium simulation. The displacement length is related to the site density, giving $\Lambda \approx n^{-1/2} = 0.30 \, \mathrm{nm}$. For the later stage of wetting we measure a slowly decreasing contact angle of around 90° on the silica. Using these numbers, we estimate the contact line speed from the molecular kinetic theory as $v_{\rm MKT} \approx 30$ m/s, which is off by one order of magnitude compared

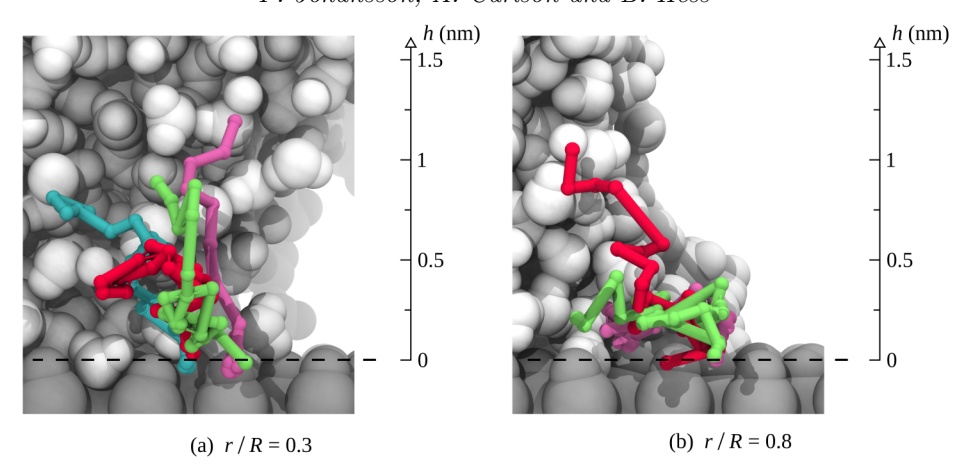


FIGURE 5. Molecular traces of selected water molecules at the contact line on a silica, at r/R of 0.3 (left) and 0.8 (right), corresponding to the sampled mass flow of figure 4a. The paths are subdivided in steps of 1 ps and show a history of 10 ps in the left figure and 20 ps in the right. (a) Molecules in the early wetting regime approach the contact line through an advective flow, coming from the droplet centre or from the droplet interface. (b) In the later regime we see a mixed process, where the majority of molecules are jumping between the potential minima of the silica substrate through a dissipative process. Only comparatively few molecules at the contact line are arriving through an advective flow from the droplet centre or interface.

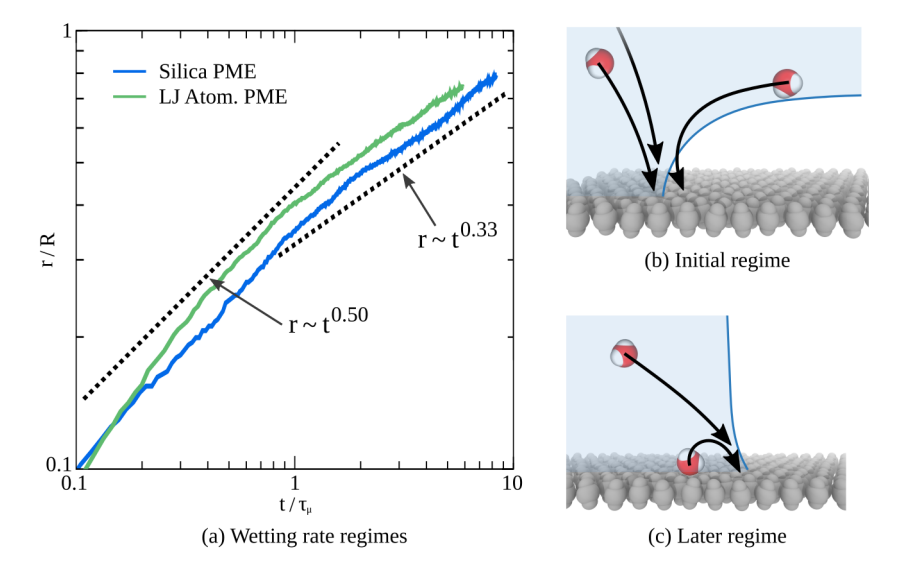


FIGURE 6. (a) The spreading radius r(t) for the PME MD simulation on the silica and the atomistic LJ substrate, represented in logarithmic coordinates to highlight two different spreading regimes. In the early regime molecules are transported to the contact line from above before a foot is formed. After the formation of the wetting foot molecules have to traverse through its geometry. To illustrate the different regimes the dotted lines show different power-laws with respect to time as $r \sim t^k$. Sketches of the molecular processes in the (b) short time initial regime and (c) the long time diffusive regime.

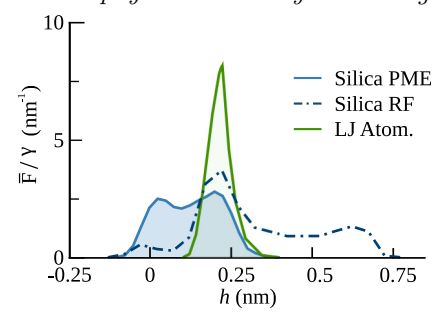
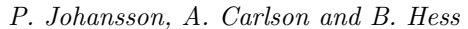


FIGURE 7. The force per area \bar{F} , scaled by the surface tension γ , which the substrates exert on a slab of liquid water separated by height h from the substrate. On the silica water molecules can penetrate the space between the upper oxygen, leading to a net force on the liquid in this region below substrate level. Although the driving force is of similar length for the atomistic LJ substrate and the silica with PME electrostatics the dynamics vary greatly, which can only be connected to the substrate topology. Reaction-field electrostatics lead to a longer interaction range for the charged silica, driving flow over three molecular layers. Note that the area under all curves equal $\gamma \cos \theta_0$.

to the MD simulation $v \approx 3$ m/s (figure 2). It is not surprising that MKT predicts a higher velocity, since κ^0 only takes the detachment of a molecule into account, not the subsequently required rearrangement of the hydrogen bonding network. For the atomistic LJ substrate, we note that although the water shows some structuring, there is only a very weak separation of sites, so rather than hopping, the water slides over the substrate which is consistent with the observed slip.

One reason for the difference in spreading rate between PME and RF electrostatics in the later stage of wetting is a modified mechanism of advancing the contact line. To clarify the different mechanisms, we use the atomistic LJ substrate as an example, which simplifies the analysis since there are no electrostatic interactions with the substrate. Visual inspection of the trajectories from MD reveal that with RF the contact line is fluctuating and rough, while it is smoother with PME. Manually counting protrusions of 1 nm size at the contact line results in about one per 20 nm for PME and one per 10 nm for RF. A Fourier analysis of the contact line fluctuations shows that it is 12 % larger for RF with a 2.3 nm wavelength. To distinguish cause from effect, we simulated a slab of water in equilibrium, confined between two LJ walls separated by 4 nm to generate a contact angle of 60°. Here we find 10 % larger Fourier components for RF compared to PME. The enhancement of fluctuations with RF is caused by a stronger electric field at the contact line, built up by the molecular electrostatics. For a liquid-vapour interface, we measured a four times stronger field with RF as with PME. With the slab geometry we observed the same factor of 4 for the field along the substrate at the contact line. Since RF uses a cut-off, the electrostatic interaction of a water dipole with the field is not four times, but twice as high with RF as with PME. This stronger interaction exponentially enhances fluctuations and in particular protrusions of water molecules out of the interface and ahead of the contact line along the substrate. The protrusions advance the contact line faster than the diffusive motion observed with PME. Although the higher fluctuations are an artifact of the RF, it shows that fluctuations can not only quantitatively affect the flow, but also qualitatively, as with RF $r(t) \propto t^{1/2}$ without a change in exponent observed with PME. This is similar to the observation Davidovitch et al. (2005) made for thin film wetting, where thermal fluctuations in the film increase the spreading rate from $r \propto t^{1/7}$ to $r \propto t^{1/4}$.

Up till now we have mainly looked at flows and source of friction. With MD we can



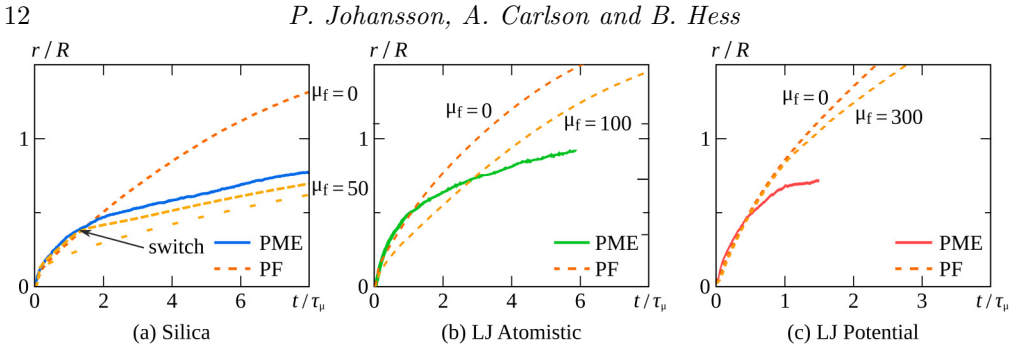


FIGURE 8. A direct comparison of the wetting dynamics predicted by the MD and the PF simulations. Wetting rates show that the short time initial regime and the long time regime of the wetting dynamics are captured by the PF model with separate friction parameters μ_f (listed in the graphs). a) To illustrate the effect of a spatially varying μ_f we use a switch, which gives a matching spreading rate between the MD and PF model. Our results suggests that at short times there is a rapid equilibration of the interface i.e. $\mu_f \sim 0$ and a long time relaxation where $\mu_f > 0$.

also quantify the different driving forces in the spreading dynamics by measuring the atomistic interaction forces at the substrate. The force working on the liquid normal to the solid substrate is evaluated as a function of the distance h from the substrate, see figure 7. We observe that the interaction range depends on the substrate type, but that it is short: 0.25-1 nm, even on the PME silica which is our most realistic substrate. This is independent of the total integrated net force, which is equal to $\gamma \cos \theta_0$ on all substrates. A strong artifact of RF electrostatics is that the force is spread over a longer distance than when using PME and water molecules are pulled from additional liquid layers. In shear flow, as observed in the later stages of the wetting dynamics, this leads to a faster flow approximately proportional to the interaction range.

4.2. Comparison between MD and PF

Next, we turn to a comparison between the PME MD spreading dynamics and the PF simulations, using the material parameters in table 2. By comparing the spreading rates for the PF simulation with $\mu_f = 0$ and the MD simulation for the different substrate, we can clearly distinguish the two different wetting regimes. At short times (r/R < 0.5)the spreading radii compares favourably between the PF and the MD simulation, while they deviate significantly at long times, as seen in figure 8. The contact line advances much faster in the PF simulations with $\mu_f = 0$ than the corresponding MD simulations. A similar observation was also made when comparing PF simulations to spreading experiments of millimetre sized water droplets (Carlson et al. 2012a,b). To obtain a match for r(t) between PF and MD we deploy a similar strategy as in (Carlson et al. 2009) and adjust the local contact line friction parameter μ_f .

Since the short time initial regime (r/R < 0.5) appears to be similar for the PF with $\mu_f = 0$ and MD, we also introduce the contact line friction from that spatial point with a switch $(1-\tanh(33(\hat{x}+0.5)))/2$ multiplying μ_f , see figure 8a. Thus, we assume that there is an initial fast relaxation, which slows down as r/R > 0.5 and $\mu_f > 0$. Introducing this spatial switch gives a good agreement between PF and MD for r(t) on silica. In a previous combined MD/PF study on a simple Lennard-Jones liquid a good match was obtained with $\mu_f = 0$ (Nakamura et al. 2013). This can be explained by the less structured liquid and the large, but not infinite, slip lengths of around half the droplet radius.

Next we turn to a comparison of the droplet shapes and the flow fields predicted by the PF and MD simulations. The first thing one notices when looking at the flow fields

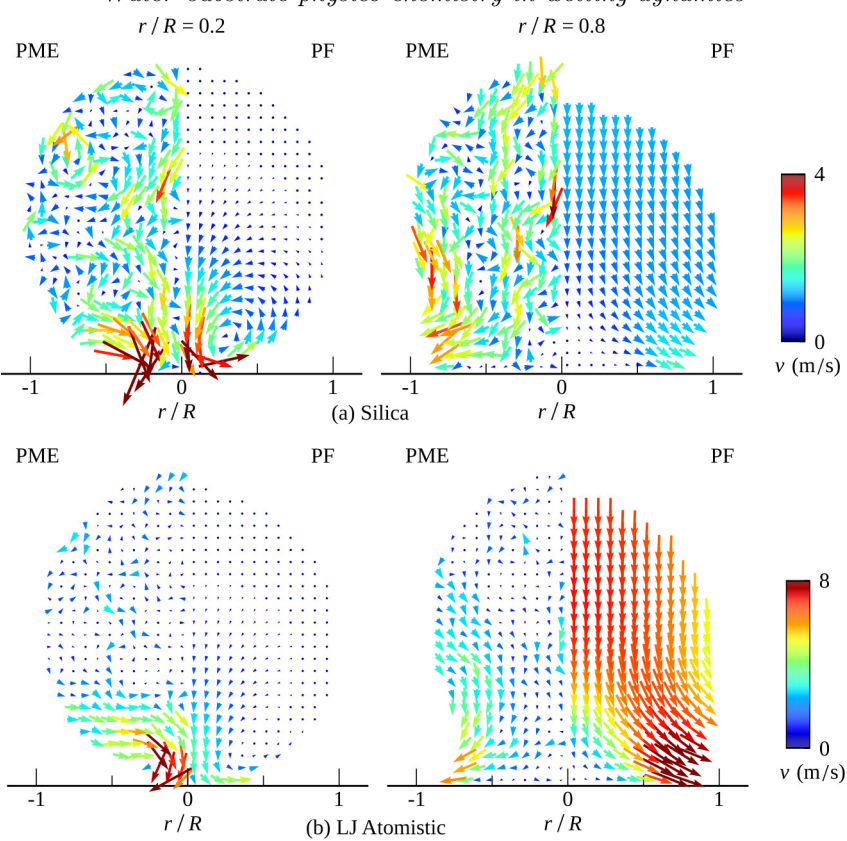


FIGURE 9. A comparison of the global flow from MD (left half of droplets) and PF simulations (right half, extracted for $\hat{C} \geqslant 0$). Shown for the early and later regimes of wetting for the atomistic substrates. To decrease thermal noise the MD flow was sampled over 300 ps for the early regime and 500 ps for the later. (a) For the silica the MD is matched against PF with the switched-on $\mu_f=50$ contact line friction factor seen in figure 8. While the wetting rates match qualitatively, the global flow is markedly different. For MD fluid is pulled in from the sides of the droplet, thinning it out. Thermal fluctuations occur on a length scale comparable to the droplet size. For PF a consistent global flow is quickly established. (b) For the atomistic LJ substrate MD is matched against PF with $\mu_f=100$. As the wetting is faster the thermal noise is decreased, and similarly to on the silica a difference in the global flow between MD and PF is observed.

in figure 9 are the thermal fluctuations in the flow visible on all length scales in the MD results, which are not present in the PF model. Although the wetting rates can be matched using the friction factor μ_f , the local dynamic contact angle differs between MD and PF simulations. Moreover, a comparison of the flow field (figure 9) illustrates that there appears to be different modes of mass transport to the contact line inside the droplet. As we have noted earlier, MD simulations indicate that the mass transport to the contact line is in the wall normal direction and from the interface area of the droplet. The continuum simulations, on the other hand, predict that the liquid is transported from the droplet centre line and along the substrate. The mismatch in flow causes a mismatch in droplet shapes where in MD the droplet initially thins from the sides by a local flow, whereas in PF the entire droplet moves towards the substrate as it spreads due to a global flow.

The different flow fields predicted in the atomistic and continuum description help us

to identify potential mechanisms that affects the dynamics. We want to highlight that the PF model is an ideal isothermal model, without any thermal fluctuations. Fluctuations might indeed be part of the reason why the flow and droplet shapes are predicted to be different for the methods. At short times, inertia dominates and molecular fluctuations are negligible in comparison, but as r(t) grows the contact line speed slows down and fluctuations start to affect the droplet dynamics. Although we noted before that fluctuations in r(t) are small when comparing different runs with the same parameters, the flow inside the droplet exhibits large fluctuations (see figure 9). Another source of discrepancy might stem from the effective material properties of the drop, which can vary in the MD simulations, in particular close to interfaces, but are fixed for the PF model.

5. Conclusion

We have combined large scale MD simulations and continuum PF theory to advance our understanding of the physical mechanisms that can influence the spreading dynamics of water droplets. To move one step closer to an experimentally realisable system, we model water droplets as they wet a silica-like substrate and compare with two simpler, unrealistic Lennard-Jones substrates. Our results demonstrate that the wetting dynamics can be significantly affected by the molecular substrate composition, even when the equilibrium contact angle is the same. The silica substrate produces a no-slip boundary condition due to strong hydrogen bonding forces between the water and the substrate molecules. This does not only lead to a slower wetting rate, but also qualitatively affects the droplet dynamics compared to the less realistic LJ substrates. We have demonstrated that the driving force for wetting on a silica monolayer has a range of a single molecular diameter, around 0.3 nm. A roughness of the substrate on this length scale can therefore effectively block the contact line from advancing and partly explains why details on the atomistic length scale can have such a large influence on the global wetting dynamics. With PME electrostatics all effective interactions are short ranged, whereas the cut-off employed in the RF electrostatics leads to artifacts at the nanometre length scale that increase the wetting rate. In particular, enhanced thermal fluctuations at the contact line qualitatively change the contact line speed. Two wetting regimes are classified within the dynamics, an initial fast wetting regime where the contact line advances through advection, followed by a slower regime where the contact line advances by a diffusive-like process.

When transferring the MD systems to a continuum description, the slip length is the only material property, among the ones we model, that changes. However, direct comparison between the MD simulations and the continuum PF simulations highlight that an additional contact line friction term is needed to match the spreading radius in time. The continuum simulations helps us identify the different wetting regimes where at short time there appears to be a rapid relaxation towards equilibrium, which is slowed down at long times. Although the spreading radius can be matched in time for the MD and PF simulations, there are discrepancies in the droplet shape and velocity profile. Part of the explanation for this discrepancy may stem from fluctuations in the MD simulations, which are not present in the continuum description. Although our droplets are large in the context of MD, they are small compared to most experimental setups. When increasing the droplet size we increase the influence of inertia, while decreasing that of large-scale thermal fluctuations. These two effects will make the MD behave more like the continuum model with a flow parallel to the solid substrate near the contact line. However, the processes at the contact line that drive the wetting dynamics are scale invariant and will therefore affect droplets of any size.

The molecular system studied here is first of its kind to blend an experimentally real-isable liquid and solid substrate together with a complete description of the electrostatic interactions, which all can have a great influence on the prediction of the droplet spreading dynamics. Our results describe the details of water as it spreads on substrates with different physico-chemistry, and highlight that there are many more question related to non-equilibrium interactions between complex liquids and solids that remain to be understood in the context of dynamic wetting.

We are grateful for stimulating discussions with G. Amberg. B. Hess thanks the Center of Smart Interfaces at the Technische Universität Darmstadt for support. This work was supported by the European Research Council (grant no. 258980) and the Swedish e-Science Research Center. Computer resources were provided through the Swedish National Infrastructure for Computing (SNIC 2014/1-30 and 2015/1-30).

REFERENCES

- ABRAHAM, M. J., MURTOLA, T., SCHULZ, R., PÁLL, S., SMITH, J. C., HESS, B. & LINDAHL, E. 2015 GROMACS: High performance molecular simulations through multi-level parallelism from laptops to supercomputers. *SoftwareX* In press, DOI: http://dx.doi.org/10.1016/j.softx.2015.06.001.
- BACHELOR, G. K. 1967 An introduction to fluid mechanics.
- BERENDSEN, H. J. C., GRIGERA, J. R. & STRAATSMA, T. P. 1987 The missing term in effective pair potentials. *Journal of Physical Chemistry* **91**, 6269–6271.
- Blake, T. D. & Haynes, J. M. 1969 Kinetics of liquid/liquid displacement. *Journal of Colloid and Interface Science* **30**, 421–423.
- Bonn, D., Eggers, J., Indekeu, J., Meunier, J. & Rolley, E. 2009 Wetting and spreading. Reviews of Modern Physics 81, 739–805.
- CAHN, J. W. & HILLIARD, J. E. 1958 Free energy of a nonuniform system. I. Interfacial free energy. *Journal of Chemical Physics* 28, 258–267.
- CARLSON, A., BELLANI, G. & AMBERG, G. 2012a Contact line dissipation in short-time dynamic wetting. Europhysics Letters 97, 44004.
- Carlson, A., Bellani, G. & Amberg, G. 2012b Universality in dynamic wetting dominated by contact line friction. *Physical Review E* 85, 045302.
- Carlson, A., Do-Quang, M. & Amberg, G. 2009 Modeling of dynamic wetting far from equilibrium. *Physics of Fluids* **21**, 121701.
- Carlson, A., Do-Quang, M. & Amberg, G. 2011 Dissipation in rapid dynamic wetting. Journal of Fluid Mechanics 682, 213–240.
- DAVIDOVITCH, B., MORO, E. & STONE, H. A. 2005 Spreading of viscous fluid drops on a solid substrate assisted by thermal fluctuations. *Physical Review Letters* **95**, 244505.
- DE CONINCK, J. & BLAKE, T. D. 2008 Wetting and molecular dynamics simulations of simple liquids. *Annual Review of Materials Research* **38**, 1–22.
- DE GENNES, P. G. 1985 Wetting: Statics and dynamics. Reviews of Modern Physics 57, 827.
- ESSMANN, U., PERERA, L., BERKOWITZ, M. L., DARDEN, T., LEE, H. & PEDERSEN, L. G. 1995 A smooth particle mesh ewald potential. J. Chem. Phys. 103, 8577–8592.
- Gentner, F., Ogonowski, G. & De Coninck, J. 2003 Forced wetting dynamics: A molecular dynamics study. *Langmuir* 19, 3996–4003.
- Ho, T. A., Papavassiliou, D. V., Lee, L. L. & Striolo, A. 2011 Liquid water can slip on a hydrophilic surface. *Proceedings of the National Academy of Sciences* **108**, 16170–16175.
- Huh, C. & Scriven, L. E. 1971 Hydrodynamic model of steady movement of a solid/liquid/fluid contact line. *Journal of Colloid and Interface Science* 35, 85.
- JACQMIN, D. 2000 Contact-line dynamics of a diffuse fluid interface. Journal of Fluid Mechanics 402, 57–88.
- Janeček, J. & Netz, R. R. 2007 Interfacial water at hydrophobic and hydrophilic surfaces: depletion versus adsorption. *Langmuir* 23, 8417–8429.

- KOPLIK, J., BANAVAR, J. R. & WILLEMSEN, J. F. 1988 Molecular dynamics of Poiseuille flow and moving contact lines. *Physical Review Letters* **60**, 1282.
- Lee, S. H. & Rossky, P. J. 1994 A comparison of the structure and dynamics of liquid water at hydrophobic and hydrophilic surfaces—a molecular dynamics simulation study. *Journal of Chemical Physics* **100**, 3334–3345.
- LIU, S., QIN, Y. & YANG, X. 2010 Molecular dynamics simulation of wetting behavior at CO₂/water/solid interfaces. Chinese Science Bulletin 66, 2252–2257.
- Nakamura, Y., Carlson, A., Amberg, G. & Shiomi, J. 2013 Dynamic wetting at the nanoscale. *Phys. Rev. E* 88 (033110).
- QIAN, T., WANG, X. P. & SHENG, P. 2003 Molecular scale contact line hydrodynamics of immiscible flows. *Physical Review E* **68**, 016306.
- QIAN, T., WANG, X. P. & SHENG, P. 2004 Power-law slip profile of the moving contact line in two-phase immiscible flows. *Physical Review Letters* 93, 094501.
- REN, W., Hu, D. & E, Weinan 2010 Continuum models for the contact line problem. *Physics of Fluids* 22, 102103.
- RITOS, K., DONGARI, N., BORG, M. K., ZHANG, Y. & REESE, J. M. 2013 Dynamics of nanoscale droplets on moving surfaces. *Langmuir* **29**, 6936–6943.
- Tanner, L. H. 1979 The spreading of silicone oil drops on horizontal surfaces. *Journal of Physics D: Applied Physics* 12, 1473.
- Thompson, P. A. & Robbins, M. O. 1989 Simulations of contact-line motion: Slip and the dynamic contact angle. *Physical Review Letters* **63**, 766.
- Voinov, O. V. 1976 Hydrodynamics of wetting. Fluid Dynamics 11, 714.
- WERDER, T., WALTHER, J. H., JAFFE, R. L., HALICIOGLU, T. & KOUMOUTSAKOS, P. 2003 On the watercarbon interaction for use in molecular dynamics simulations of graphite and carbon nanotubes. *The Journal of Physical Chemistry B* **107**, 1345–1352.
- Winkels, K. G., Weijs, J. H., Eddi, A. & Snoeijer, J. H. 2012 Initial spreading of low-viscosity drops on partially wetting surfaces. *Physical Review E* 85, 055301.
- Young, T. 1805 An essay on the cohesion of fluids. *Philosophical Transactions of the Royal Society of London* **95**, 65–87.
- Yue, P., Zhou, C. & Feng, J. J. 2010 Sharp-interface limit of the Cahn-Hilliard model for moving contact lines. *Journal of Fluid Mechanics* 645, 279–294.